Mixed Conducting Ceramic Hollow-Fiber Membranes for Air Separation

Xiaoyao Tan, Yutie Liu, and K. Li
Dept. of Chemical Engineering and Chemical Technology, Imperial College London, University of London, South Kensington, U.K. SW7 2AZ

DOI 10.1002/aic.10475
Published online May 9, 2005 in Wiley InterScience (www.interscience.wiley.com).

Mixed conducting ceramic hollow-fiber membranes, which possess an asymmetric structure, were prepared by a combined phase inversion and sintering technique where precursors of the hollow fibers were first spun using a polymer solution containing suspended LSCF powders and were then sintered at elevated temperature. By controlling the weight ratio of the LSCF powder to the polymer binder, sintering temperature, and time, the LSCF hollow fibers with gastight properties have been prepared and evaluated using an apparatus developed during the course of this study. Using the gastight LSCF hollow fibers, a membrane module was assembled for air separation. The performances of the module for air separation have been studied under various operating modes and at different temperatures and feed flow rates both experimentally and theoretically. The results reveal that the surface exchange reaction at the downstream side is much more important than that at the upstream side, especially for lower operating temperatures. The porous inner surface of the prepared LSCF hollow-fiber membranes substantially favors the oxygen permeation when air is fed in the shell side of the membrane module. At high operating temperatures, oxygen permeation can be enhanced by the countercurrent flow operation. Vacuum operation favors the oxygen permeation kinetically in the LSCF hollow-fiber membrane modules. © 2005 American Institute of Chemical Engineers *AIChE J,* 51: 1991–2000, 2005

Keywords: air separation, mixed conducting ceramic, hollow-fiber membrane module, perovskite membrane

Introduction

It is generally believed that some perovskite ceramics such as $La_{1-x}Sr_xCo_{1-y}Fe_yO_{3-\alpha}$ (LSCF) exhibit a good mixed ionic-electronic conducting property.[1-5] Dense membranes prepared from these ceramic materials show good oxygen permeation at elevated temperatures without the need of external electrical loadings. Furthermore, because no species other than oxygen can be transferred through the membrane, the oxygen permselectivity is theoretically infinite. As a result, pure oxygen production can be achieved by heating such a ceramic membrane system (or oxygen generator) where air is used as a feedstock. To develop the membrane system for industrial use, it is essential to improve not only the oxygen permeation flux of the membrane materials, but also the membrane systems, which are stable in harsh environments.

Many efforts have been made so far to improve oxygen permeation fluxes of perovskite membranes. Oxygen permeation through a dense perovskite membrane is controlled by the oxygen diffusion rate in the membrane as well as the surface oxygen exchange kinetics on either side of the membrane.[5,6] Therefore, it is generally expected that the oxygen flux can be improved once the membrane thickness is reduced[7] or the surface of the membrane is modified, that is, application of porous catalytic layers on either side or both sides of the membrane, leading to an enhancement of surface oxygen-exchange kinetics.[8-10]

Correspondence concerning this article should be addressed to K. Li at Kang.Li@Imperial.ac.uk.

Table 1. Parameters for Preparing LSCF Hollow-Fiber Membranes

Parameter	Value
Starting solution composition (wt %)	
LSCF powder	70.49
PESf, Radel A-300	5.81
NMP	23.26
PVP K30	0.44
Dope temperature (°C)	20
Internal coagulant temperature (°C)	20
Injection rate of internal coagulant (mL/min)	9.5
Nitrogen pressure (atm)	0.5
Air gap (cm)	1.0
Sintering temperature (°C)	1280
Sintering time (h)	4

In addition, the membrane configuration such as flat sheet, tubular, or hollow fiber also plays an important role in the overall ceramic membrane systems for air separation. In most previous studies, disc-shaped membranes with only a limited membrane area (<5 cm^2) were usually used because they are easily fabricated using conventional static-pressing methods. Although a multiple planar stack can be adopted to enlarge the membrane area to a plant scale, many problems such as high-temperature sealing, connection, and pressure resistance have to be faced.[3] Tubular perovskite membranes were developed to reduce the engineering difficulties, especially the problem associated with high-temperature sealing,[11,12] although their small surface area/volume ratio and the high membrane thickness, which would lead to low oxygen permeation rates, make them unfavorable in practical applications.

Recently, hollow-fiber ceramic membranes with an asymmetric structure have been successfully prepared using a phase-inversion spinning/sintering technique.[13-15] Compared to the disk-shaped membranes, such hollow-fiber membranes possess much larger membrane area per unit volume for oxygen permeation. By adopting long hollow fibers and keeping the two sealing ends away from the high-temperature zone, the problem of high-temperature sealing no longer exists. Furthermore, because of the asymmetric structure (that is, a thin separating dense layer integrated with porous layers on either side or both sides), the membrane's resistance to oxygen permeation is substantially reduced compared to that of symmetric membranes prepared by conventional methods. In addition, the integrated porous layers on either side or both sides of the membrane also provide much larger gas–membrane interfaces for oxygen-exchange reactions, leading to an enhancement of surface oxygen-exchange kinetics and thus to an improved oxygen permeation rate. All these advantages of the ceramic membrane in asymmetric and hollow-fiber configurations would, in the foreseeable future, position the perovskite mixed conducting membranes into commercial applications.

In this study, LSCF hollow-fiber membranes have been prepared by a combined phase-inversion spinning/sintering technique. A membrane module consisting of six dense LSCF hollow fibers has been fabricated for air separation. The performances of the membrane module for air separation at different operating modes, operating temperatures, and feed flow rates have also been investigated both experimentally and theoretically.

Experimental

Preparation of LSCF hollow-fiber membranes

LSCF hollow-fiber membranes were prepared using a combined phase-inversion/sintering technique. The detailed preparation procedures are described elsewhere.[14] In this work, the starting solution consisted of 70.49 wt % LSCF powders, 5.81 wt % polyethersulfone (PESf), 23.26 wt % 1-methyl-2-pyrrolidinone (NMP), and 0.44% polyvinyl pyrrolidone (PVP, K30). The membrane precursors were calcined at 1280°C for 4 h, followed by a gastight test as described below. The parameters used to prepare the LSCF hollow-fiber membranes are summarized in Table 1.

Gastightness of the hollow-fiber membranes

Gastightness of the prepared hollow-fiber membranes was tested using a gas permeation apparatus, as shown schematically in Figure 1. The hollow-fiber membrane for the test was glued onto a stainless steel sample holder with an epoxy resin (UKR-135 resin with UKH-136 hardener; UK Epoxy Resins, Lancashire, UK). It was then assembled into a cylinder with a volume capacity of 500 cm^3). Nitrogen was used as a test gas. The pressure change with time of the cylinder was measured with a pressure transducer (Model PX300–050GV; Omega Engineering Inc., Stamford, CT) attached to the test cylinder and was recorded through a panel meter (Model DP25B-S, supplied by Omega Engineering Inc.). The gas permeance is thus obtained based on the cylinder pressure change with time:

$$P = \frac{V}{RT \cdot A_m t} \ln\left(\frac{p_0 - p_a}{p_t - p_a}\right) \tag{1}$$

where P is the permeance of the test membrane (mol m^{-2} s^{-1} Pa^{-1}); V is the volume of the test cylinder (m^3); R is the gas constant (8.314 J mol^{-1} K^{-1}); and T is the measured temperature (K). p_0 and p_t are the initial and final measured pressures in the test cylinder (Pa); p_a is the atmospheric pressure (Pa). A_m (m^2) is the membrane area, that is, $A_m = [2\pi(R_o - R_{in})L]/\ln(R_o/R_{in})$, where R_o and R_{in} are, respectively, the outer and the inner radius of the hollow fiber (m); L is the length of the hollow-fiber membrane (m); and t is the time for measurement (s). If the nitrogen permeance measured is $<10^{-10}$ mol m^{-2} Pa^{-1} s^{-1}, the membrane may be considered to be gastight.

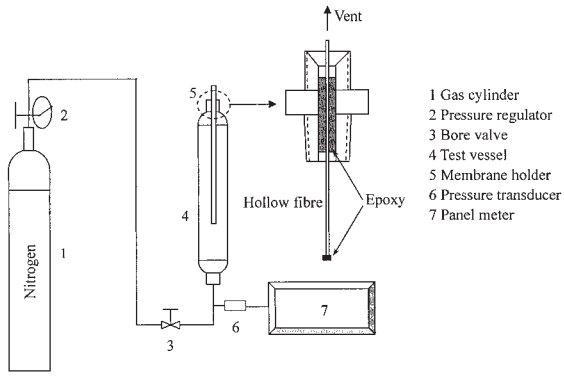

Figure 1. Experimental setup for gastightness test.

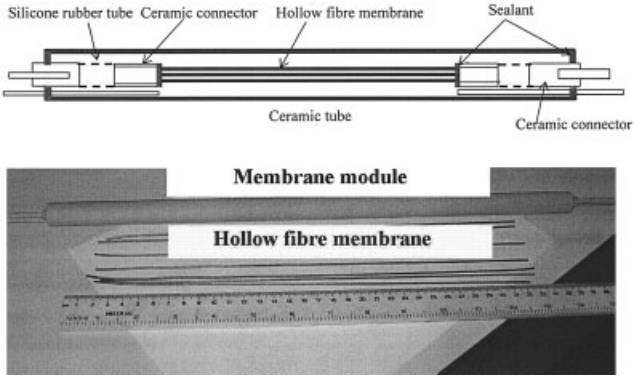

Figure 2. Configuration of the LSCF hollow-fiber membrane module.

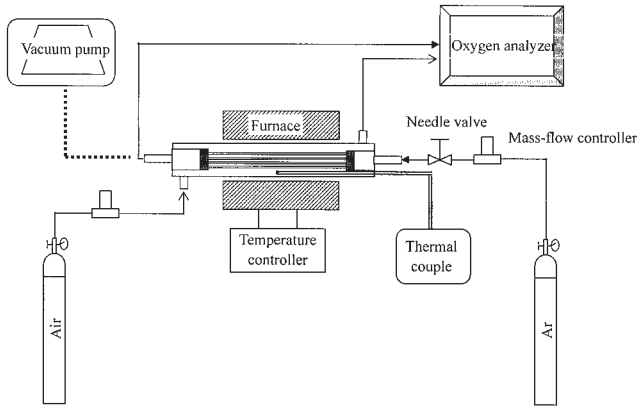

Figure 3. Experimental setup for air separation.

Fabrication of the LSCF hollow-fiber membrane module

Although problems of high-temperature sealing can be avoided using a long hollow-fiber membrane,[14] the thermal expansion of the fibers must also be taken into consideration. It was found that the LSCF hollow-fiber membrane would break into pieces at temperatures $> 500°C$ if both ends of the fiber were fixed with the module shell. Therefore, in this work, soft silicone rubber tubes were used to offset the thermal expansion of the hollow-fiber membranes. Figure 2 shows the characteristics of the prepared membrane module as well as the LSCF hollow fibers. As can be seen in Figure 2, two ends of the LSCF hollow-fiber membranes were indirectly glued onto the module shell by flexible silicone rubber tubes and ceramic connectors. The sealant used for the module is the high-temperature–resistant adhesive Light® (Fortafix Ltd., Peterborough, UK). Values of the characteristic parameters of the prepared LSFC hollow-fiber membrane module are given in Table 2.

Air separation using the LSCF hollow-fiber membrane module

The experimental setup for air separation in the LSCF hollow-fiber membrane module is shown in Figure 3. The membrane module was placed in a Carbolite® tubular furnace with the length of 15 cm. Thus, the sealing joints were kept 6 cm away from the inlet of the furnace tube. Before experiments, the temperature profile within the module (inside the alumina tube) was measured using a type C thermocouple with a thermometer supplied by Omega Engineering Inc. The feed gas flow rates were controlled and measured using a mass flow controller (Smart Mass flow meter with read out and control electronics; Model 0152, Brooks Instruments, Newcastle upon Tyne, UK). Argon was used as a sweep gas and was introduced either in the shell side (lumen-feed mode) or in the fiber lumen (shell-feed mode). In the vacuum operation, a self-cleaning dry vacuum system (Model 2025; Welch Rietschle Thomas, Skokie, IL) was applied to the fiber lumen while the air stream was flowing through the shell side. Oxygen concentrations in both the air stream and the argon stream effluents were measured online using an oxygen meter (Oxygen Analyser 572; Servomex, East Sussex, UK). The overall oxygen permeation rate is calculated from the concentration changes of oxygen in the argon stream or in the air stream:

From the Argon Stream

$$N_t = \frac{F_{\mathrm{Ar}} y_e}{(1 - y_e)} \tag{2a}$$

From the Air Stream

$$N_t = \frac{F_{\mathrm{Air}}(0.21 - x_e)}{(1 - x_e)} \tag{2b}$$

where F is the feed gas flow rate (mol/s); x_e and y_e are, respectively, oxygen concentrations in the air or in the argon effluents.

Table 2. Properties of the Hollow-Fiber Membrane Module

Property	Value
OD of the hollow-fiber membranes	1.46 mm
ID of the hollow-fiber membranes	1.14 mm
Number of the hollow-fiber membranes	6
Length of the hollow-fiber membranes	27 cm
ID of the alumina tube	1.4 cm
OD of the alumina tube	1.8 cm
Total length of the module	40 cm
Length of the silicone rubber tube	4.0 cm
Packing density of fibers	3.95%

Theory

Oxygen permeation rate through a hollow-fiber membrane

Oxygen permeation through a mixed ionic-electronic conducting perovskite membrane may not be controlled solely by the oxygen diffusion rate (or the diffusion rate of oxygen vacancy) in the membrane, but also by the surface oxygen-exchange kinetics on both sides of the membrane.[5,6] The local oxygen permeation rate through a hollow-fiber (or tubular) membrane can be given as[16]

$$\frac{dN_{\mathrm{O_2}}}{dl} = \frac{k_r[(p'_{\mathrm{O_2}})^{0.5} - (p''_{\mathrm{O_2}})^{0.5}]}{\dfrac{(p''_{\mathrm{O_2}})^{0.5}}{2\pi R_o} + \dfrac{k_f \ln(R_o/R_{in})(p'_{\mathrm{O_2}})^{0.5}(p''_{\mathrm{O_2}})^{0.5}}{\pi D_V} + \dfrac{(p'_{\mathrm{O_2}})^{0.5}}{2\pi R_{in}}} \tag{3}$$

It can be seen that the total permeation resistance consists of three parts: (1) the exchange reaction at the outer membrane surface (shell side), (2) bulk diffusion, and (3) the exchange reaction at the inner membrane surface (lumen side). The above equation can be simplified if one or two steps of the resistances are negligible. For example, if the oxygen permeation is controlled by outer surface exchange and bulk diffusion, Eq. 3 then reduces to

$$\frac{dN_{O_2}}{dl} = \frac{k_r[(p'_{O_2})^{0.5} - (p''_{O_2})^{0.5}]}{\frac{(p''_{O_2})^{0.5}}{2\pi R_o} + \frac{k_f \ln(R_o/R_{in})(p'_{O_2})^{0.5}(p''_{O_2})^{0.5}}{\pi D_V}} \tag{3a}$$

If the outer surface exchange is negligible, the Eq. 3 then reduces to

$$\frac{dN_{O_2}}{dl} = \frac{k_r[(p'_{O_2})^{0.5} - (p''_{O_2})^{0.5}]}{\frac{k_f \ln(R_o/R_{in})(p'_{O_2})^{0.5}(p''_{O_2})^{0.5}}{\pi D_V} + \frac{(p'_{O_2})^{0.5}}{2\pi R_{in}}} \tag{3b}$$

In the above equations, N_{O_2} is the oxygen permeation molar flow rate (mol/s). p'_{O_2} and p''_{O_2} are the oxygen partial pressures in the shell and the lumen side, respectively (Pa); D_V is the diffusion coefficient of oxygen vacancy (m^2/s). k_f and k_r are, respectively, the forward and the reverse reaction rate constants for the surface exchange reaction

$$0.5O_2 + V_O^{\bullet\bullet} \overset{k_f/k_r}{\longleftrightarrow} O_O^x + 2h_i^{\bullet} \tag{4}$$

where the charged defects are defined using the Kröger–Vink notation. That is, O_O^x stands for lattice oxygen, $V_O^{\bullet\bullet}$ for oxygen vacancy, and $h_i^{\bullet}$ for the electron hole.

It should be noted that Eq. 3 is suitable for both the shell-feed and the lumen-feed operating modes. In the lumen-feed operation, the local oxygen permeation rate is negative, which means oxygen permeates from lumen to shell.

Models for air separation in a hollow-fiber membrane module

Models for air separation in a membrane module consisting of m LSCF hollow fibers are developed below, which depend on the practical operating modes, as schematically illustrated in Figure 4. In the formulation of mathematical models, the following general assumptions have been made:

(1) Mass transfer resistance in the gas phase is negligible.

(2) Gas streams in the shell side and in the lumen are both plug flow.

(3) The transfer of charged defects (oxygen vacancy and electron) in the membrane occurs only in the radial direction of the membrane.

(4) Both the diffusion coefficient of oxygen vacancy and the surface exchange rate constants are independent of oxygen partial pressures.

(5) The ideal gas law is applicable to describe the gas behavior of both single component and gas mixture.

(6) The operation runs at steady state.

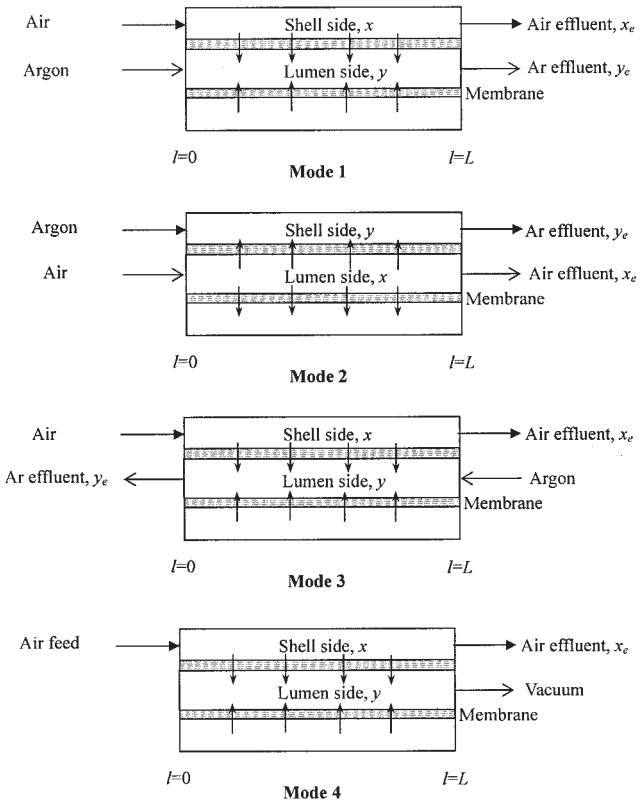

Figure 4. Operating modes of the membrane module for air separation.

Mode 1: Shell-Feed, Cocurrent Flow Operation. In this operating mode, air is introduced into the shell side of the module, while argon is cocurrently fed into the fiber lumen. The material balance equations for the shell and lumen gas streams are given, respectively, as:

- Shell side for oxygen

$$\frac{d}{dl}\left(\frac{p'_{O_2}\upsilon_s}{RT}\right) = -m\frac{dN_{O_2}}{dl} \tag{5a}$$

- Shell side for nitrogen

$$\frac{(p_s - p'_{O_2})\upsilon_s}{RT} = 0.79F_{Air} \tag{5b}$$

- Lumen side for oxygen

$$\frac{d}{dl}\left(\frac{p''_{O_2}\upsilon_l}{RT}\right) = m\frac{dN_{O_2}}{dl} \tag{6a}$$

- Lumen side for argon

$$\frac{(p_l - p''_{O_2})\upsilon_l}{RT} = F_{Ar} \tag{6b}$$

with the following boundary conditions:

$$l = 0 \qquad p'_{O_2} = 0.21p_a \qquad p''_{O_2} = 0 \tag{7}$$

where v_l and v_s are the volumetric flow rates of the lumen and the shell gas streams, respectively (m^3/s). p_l and p_s are, respectively, the pressures in the fiber lumen and the shell side, and equal to atmosphere pressure (that is, 1.013×10^5 Pa).

Mode 2: Lumen-Feed, Cocurrent Flow Operation. This operating mode shows that air is introduced into the fiber lumen, whereas argon flows cocurrently in the shell side of the module.

- Shell side for oxygen

$$\frac{d}{dl}\left(\frac{p'_{O_2}v_s}{RT}\right) = -m\frac{dN_{O_2}}{dl} \tag{8a}$$

- Shell side for argon

$$\frac{(p_s - p'_{O_2})v_s}{RT} = F_{Ar} \tag{8b}$$

- Lumen side for oxygen

$$\frac{d}{dl}\left(\frac{p''_{O_2}v_l}{RT}\right) = m\frac{dN_{O_2}}{dl} \tag{9a}$$

- Lumen side for nitrogen

$$\frac{(p_l - p''_{O_2})v_l}{RT} = 0.79F_{Air} \tag{9b}$$

with the following boundary conditions:

$$l = 0 \qquad p'_{O_2} = 0 \qquad p''_{O_2} = 0.21p_a \tag{10}$$

Mode 3: Shell-Feed, Countercurrent Flow Operation. In this operating mode, air is introduced into the shell side of the module, whereas argon is fed into the fiber lumen from the opposite end of the feed air inlet. The governing equations for this operation are as follows:

- Shell side for oxygen

$$\frac{d}{dl}\left(\frac{p'_{O_2}v_s}{RT}\right) = -m\frac{dN_{O_2}}{dl} \tag{11a}$$

- Shell side for nitrogen

$$\frac{(p_s - p'_{O_2})v_s}{RT} = 0.79F_{Air} \tag{11b}$$

- Lumen side for oxygen

$$\frac{d}{dl}\left(\frac{p''_{O_2}v_l}{RT}\right) = -m\frac{dN_{O_2}}{dl} \tag{12a}$$

- Lumen side for argon

$$\frac{(p_l - p''_{O_2})v_l}{RT} = F_{Ar} \tag{12b}$$

with the following boundary conditions:

$$l = 0 \qquad p'_{O_2} = 0.21p_a \qquad l = L \qquad p''_{O_2} = 0 \tag{13}$$

where L is the membrane's length in the furnace tube (m).

Mode 4: Shell-Feed, Cocurrent Flow with Vacuum Operation. In this operation, air flows in the shell side of the module, whereas a vacuum is applied to the fiber lumen side at the same end of the module as the air effluent outlet. The mass conservation equations on the shell side are as follows:

- Shell side for oxygen

$$\frac{d}{dl}\left(\frac{p'_{O_2}v_s}{RT}\right) = -m\frac{dN_{O_2}}{dl} \tag{14a}$$

- Shell side for nitrogen

$$\frac{(p_s - p'_{O_2})v_s}{RT} = 0.79F_{Air} \tag{14b}$$

On the lumen side, the gas stream is pure oxygen:

$$\frac{d}{dl}\left(\frac{p''_{O_2}v_l}{RT}\right) = m\frac{dN_{O_2}}{dl} \tag{15}$$

For vacuum operation, pressure drop may occur in the fiber lumen. The Hagen–Poiseuille equation can be used to describe the oxygen pressure profile in the lumen for laminar flow:

$$\frac{dp''_{O_2}}{dl} = -\frac{8\mu v_l}{m\pi R_{in}^4} \tag{16}$$

with the following boundary conditions:

$$l = 0 \qquad p'_{O_2} = 0.21p_a \qquad v_l = 0 \qquad l = L \qquad p''_{O_2} = p_v \tag{17}$$

where μ is the viscosity of oxygen (Pa·s) and p_v is the operating vacuum level (absolute pressure; Pa).

As can be seen, the governing equations for each operating mode are a group of ordinary differential equations, and thus can be solved numerically using the Runge–Kutta method.

Results and Discussion

Membrane structure

Figure 5 shows SEM microphotographs of the prepared LSCF hollow-fiber membrane before and after sintering. It can readily be seen that the asymmetric structure has been formed in the process of spinning, as shown in Figure 5A. After sintering, the asymmetric structure is retained, but with the change in voids stemming from shrinkage, as shown in Figure 5B. The membrane outer surface shown in Figure 5C indicates

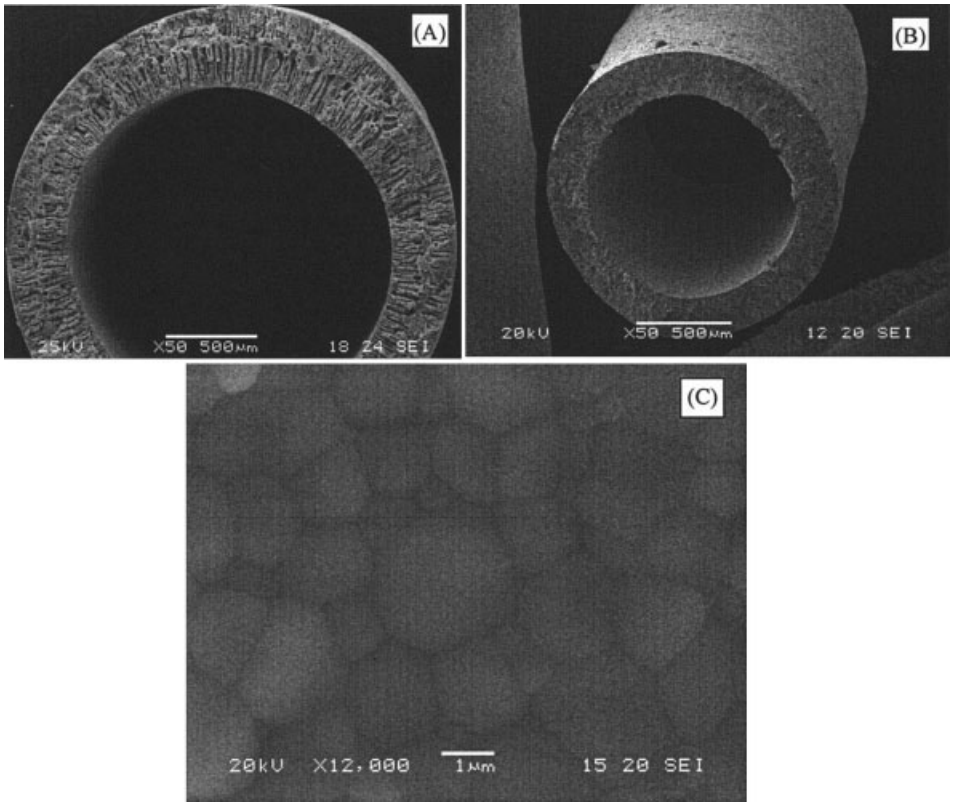

Figure 5. SEM micrographs of the LSCF hollow fiber.

(A) before sintering; (B) after sintering; (C) membrane surface.

that the LSCF particles are closely connected to each other with clear boundaries. After sintering at 1280°C for 4 h such membranes become gastight, which is confirmed using a gas permeation test described above.

Figure 6 compares the X-ray diffraction (XRD) patterns of the sintered membranes with the original LSCF powders. As can be seen, no changes are observed in the crystalline structure of the LSCF material resulting from the spinning and sintering processes after the hollow-fiber membranes are formed. However, the intensity of the corresponding characteristic peaks for the hollow-fiber membranes is much higher than that for the original LSCF powders, which suggests that the crystalline in the membranes has become larger after sintering at high temperatures.

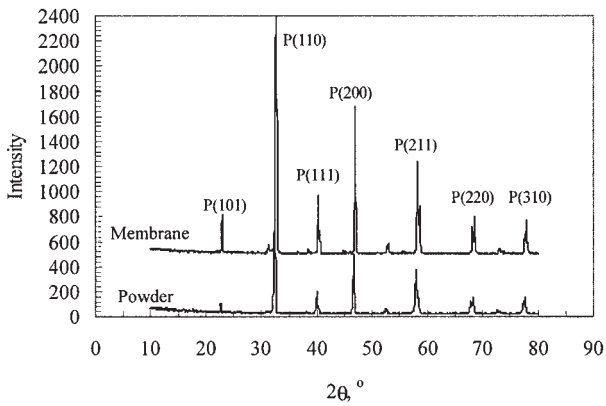

Figure 6. XRD patterns of the LSCF powder and of the sintered hollow-fiber membrane.

Gastightness of the hollow-fiber membranes

As has been well established, the perovskite membranes for oxygen permeation must be gastight without any defects. The gastight test was conducted for all the hollow fibers in the membrane module. Figure 7 illustrates a typical result of one of the hollow fibers, where the pressure in the test cylinder is plotted against the time. The gas permeance of the fiber was calculated according to Eq. 1 and was found to be 2.82×10^{-10} mol m^{-2} Pa^{-1} s^{-1}. This value is much lower than the oxygen permeability through the hollow fibers at elevated temperatures (estimated to be 2.2×10^{-4} mol m^{-2} Pa^{-1} s^{-1} at 800°C, which

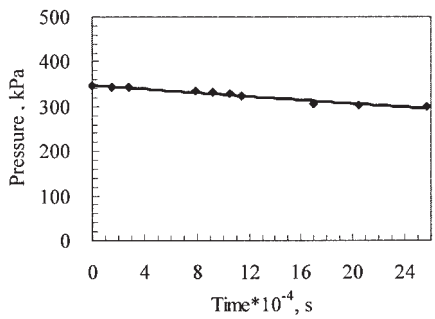

Figure 7. Pressure change with time in the gastightness test of hollow-fiber membranes.

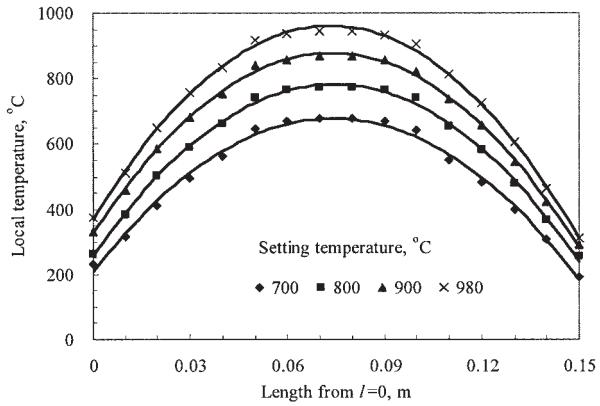

Figure 8. Temperature profile in the membrane module.

is described in detail in the following section). It should be noted that a slight decrease in pressure in the test cylinder is a result of not only the negligible gas permeation through the membrane, but also the possible leak from joints of the system. Therefore, the actual permeance arising from the leakage of the fiber is even lower than the above-calculated result and the hollow fiber of the membrane module is thus considered to be gastight.

Temperature profile in the membrane module

The temperature-uniform zone of the furnace given by the manufacturer is only 4.0 cm in length. However, the actual length of the hollow-fiber membranes for oxygen permeation should be different depending on the temperature settings. Because any parts of the hollow-fiber membranes where the temperature is high enough are able to contribute to oxygen permeation, it is necessary to know the actual temperature profile in the membrane module so as to accurately analyze the experimental data. Figure 8 illustrates the temperature profile of the furnace at a given temperature. It can be seen that the actual temperature in the temperature-uniform zone for air separation is lower than the setting value because of the insulation effect of ceramic tube. By use of least-square regression, a correlation is obtained with an R^2 value of 0.998

$$T = -(0.0086T_s + 2.5621)l^2 + (0.1201T_s + 43.46)l + (0.5854T_s - 205.59) + 273 \quad (18)$$

where T_s is the setting value (°C).

Obviously, the higher the setting temperature, the larger the membrane area provided for oxygen permeation in the module. In the following simulations, the temperature profile or Eq. 18 is incorporated into the modeling equations. However, for the purpose of illustration, the furnace setting temperature will be depicted in the subsequent figures.

Air separation results

Figure 9 shows experimental and theoretical results for the shell-feed and cocurrent flow operation where the oxygen permeation rate is plotted against the argon or air flow rates at different operating temperatures. In Figure 9A, the effect of argon flow rate on oxygen permeation rate is illustrated, keeping airflow rate constant at 24.1 cm^3/min. As expected, the oxygen permeation rate increases with increasing argon flow rate because the oxygen partial pressure in the downstream decreases as the argon flow rate is increased, thus promoting an increased driving force for oxygen permeation. In Figure 9B, the effect of airflow rate on oxygen permeation is depicted with the argon flow rate kept constant at 32.4 cm^3/min for 800°C, and at 64.5 cm^3/min for 850 and 900°C, respectively. It can be seen that effect of airflow rate on the oxygen permeation is generally negligible, especially at low temperatures, because for the operating conditions used, the amount of oxygen permeated is small compared to the amount of oxygen introduced into the module. Therefore, the oxygen driving force—and thus the oxygen permeation rate—remains relatively unchanged. As the operating temperature increases, the effect of airflow on oxygen permeation rate becomes noticeable, indicating that the operating temperature plays a more important role than the oxygen driving force in oxygen permeation.

In Figure 9, modeling results using literature kinetic parameters obtained from a disc-shaped symmetric membrane[6] are also plotted in solid lines and compared with the experimental data. As can be seen, both experimental and modeling results show the same trend. However, the experimental results are better than the modeling ones except for the operating temperature of 900°C. This difference may be attributed to the different membrane surface structure because the LSCF hollow-fiber membranes prepared using the phase-inversion/sintering technique possess an asymmetric structure where the inner

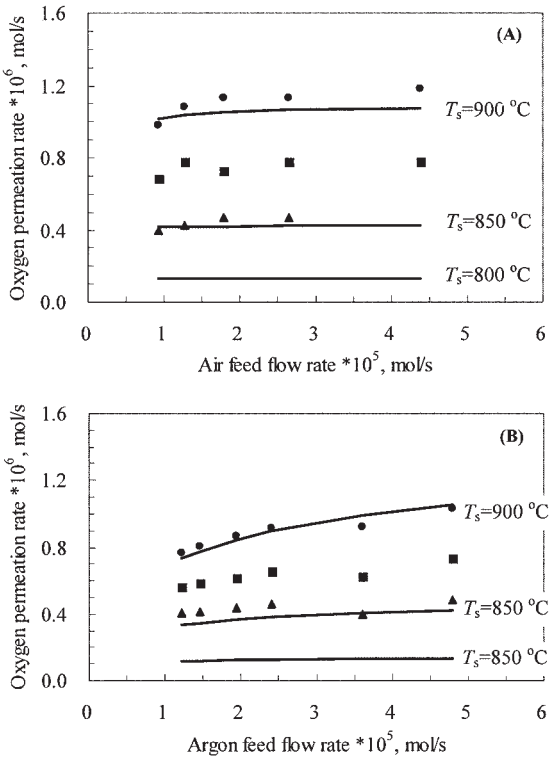

Figure 9. Oxygen permeation rate as a function of the gas flow rate for the shell-feed and cocurrent operating mode.

(A) Air feed flow rate is constant; (B) argon feed flow rate is constant. Experimental data: ▲, 800°C; ■, 850°C; ●, 900°C.

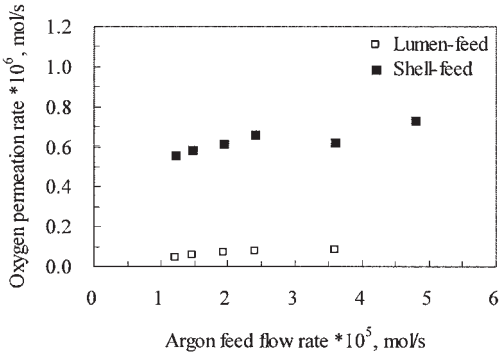

Figure 10. Comparison between the lumen-feed and shell-feed operations.

T_s = 850°C.

surface layer of the membranes is porous and thus the membrane area for the surface exchange reaction is higher than that of the symmetric membrane.[6] Therefore, the downstream surface exchange resistance is substantially decreased because of the higher surface area. As a result, the experimental results are better than modeling values at lower temperatures where the downstream surface exchange is, in general, the controlling step (which is further illustrated theoretically in Figure 11). As the temperature increases, the bulk diffusion plays an increasingly important role in oxygen permeation and gradually becomes the controlling step. Therefore, the enhancement of oxygen permeation resulting from the better membrane surface structure would be diminished as the operating temperature

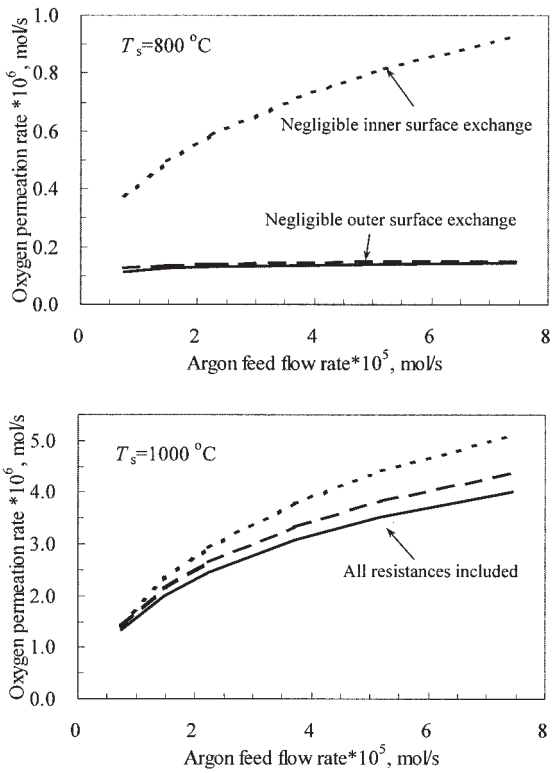

Figure 11. Modeling results for the shell-feed, cocurrent flow operation at different temperatures.

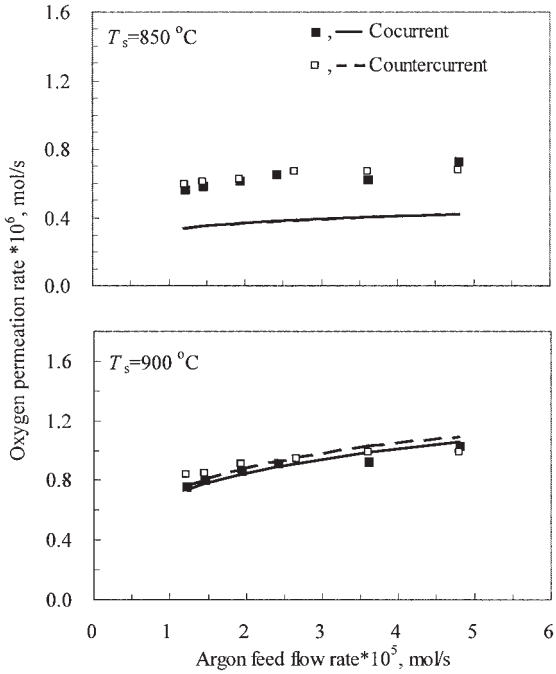

Figure 12. Comparison between the countercurrent and cocurrent flow patterns.

increases; thus the experimental data are close to the modeling results (900°C).

Figure 10 compares the results between the lumen-feed operation and the shell-feed operation at 850°C. As can be seen, the experimental data for the lumen-feed operation are substantially inferior to data obtained from the shell-feed operation, further confirming that the downstream surface exchange kinetics assumes the primary role in oxygen permeation at low operating temperatures.

Figure 11 theoretically illustrates the importance of each resistance (upstream surface exchange, bulk diffusion, and downstream surface exchange) for oxygen permeation at 800 and 1000°C, respectively. It can be seen that at the low operating temperature (that is, 800°C), the upstream surface exchange resistance shows a negligible effect, given that the simulation results obtained without considering upstream surface exchange resistance (dashed line) overlap with the solid line calculated for the actual case, that is, considering all three resistances. Because the downstream surface exchange resistance is assumed to be negligible, the oxygen permeation rate (dotted line) is considerably higher, suggesting that the downstream surface exchange is the controlling step for oxygen permeation. When the temperature is elevated to 1000°C, the difference is dramatically reduced, which indicates that the contribution of the downstream surface exchange to the overall resistance becomes small at high temperatures, and the bulk diffusion gradually becomes the controlling step.

Figure 12 compares the results between countercurrent flow and cocurrent flow patterns at two different temperatures for the shell-feed operation. Both the experimental and modeling results indicate that the oxygen permeation rate in the countercurrent flow operation is slightly higher than that in the cocurrent flow operation, a phenomenon explained by the fact that the permeation driving force in countercurrent flow is larger

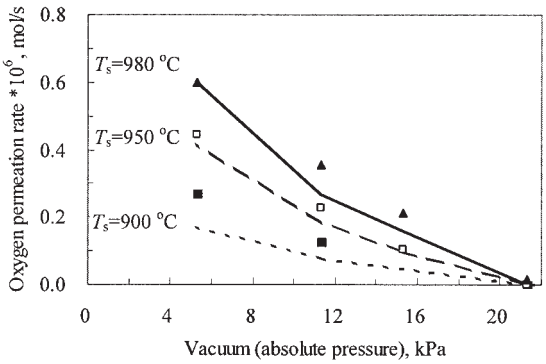

Figure 13. Oxygen permeation rate against vacuum level (absolute pressure).

than that in cocurrent flow, although the difference is not so noticeable as expected. At low operating temperature, the experimental data are better than the modeling values because of the asymmetric structure of the membrane developed. A more positive effect of countercurrent flow on oxygen permeation at high temperatures than that at lower temperatures can be expected, as shown in Figure 12, because the bulk diffusion plays an increasingly important role in permeation as the temperature increases.

The effect of the vacuum level on the performance of the membrane module is given in Figure 13, where the oxygen permeation rate is plotted against the absolute pressures at different operating temperatures. In this experiment, air flows in the shell side of the module whereas the vacuum is applied to the fiber lumen at the same end of the module as the air effluent outlet. As expected, the oxygen permeation rate increases as the applied vacuum level is increased (that is, the absolute pressure is decreased). The theoretical results are also plotted in the figure with the solid curves. It can be seen that the experimental data are in good agreement with modeling results. Unlike the sweep gas operation, the experimental data are greater than the corresponding modeling values in the vacuum operation. This may be attributable to the fact that the oxygen molecules in the inner porous layer (downstream) are able to be released easily from the membrane surface under vacuum operation. Conclusively, the vacuum operation favors the oxygen permeation kinetically in the LSCF hollow-fiber membrane modules.

Conclusions

Gastight LSCF hollow-fiber membranes that possess an asymmetric structure have been prepared by phase-inversion spinning, followed by sintering at 1280°C for 4 h. Using the prepared LSCF hollow-fiber membranes, a membrane module was designed and fabricated for air separation. For oxygen permeation, the downstream surface exchange plays an important role compared to the upstream surface exchange, especially at low operating temperatures. The porous inner surfaces of the prepared LSCF hollow-fiber membranes substantially favor oxygen permeation when air is fed into the shell side of the membrane module. At high temperatures, oxygen permeation can be enhanced by the countercurrent flow operation. Vacuum operation favors the oxygen permeation kinetically in the LSCF hollow-fiber membrane modules.

Acknowledgments

The authors gratefully acknowledge the research funding provided by The Engineering and Physical Sciences Research Council (EPSRC) in the United Kingdom (Grant No. GR/S12203).

Notation

A_m = membrane area, $A_m = [2\pi(R_o - R_{in})L]/\ln(R_o/R_{in})$, m^2
D_V = effective diffusivity of oxygen vacancy, m^2/s
F = feed gas flow rate, mol/s
k_r = reverse surface reaction rate constant of Eq. 4, mol m^{-2} s^{-1}
k_f = forward surface reaction rate constant of Eq. 4, m $Pa^{-0.5}$ s^{-1}
l = variable length of hollow-fiber membrane, m
L = length of hollow-fiber membrane, m
m = number of hollow-fiber membranes
N_{O_2} = oxygen permeation molar flow rate, mol/s
P = gas permeance of membrane, mol m^{-2} s^{-1} Pa^{-1}
p_t = pressure at t, Pa
p_0 = initial pressures in the test cylinder, Pa
p_a = atmospheric pressure, 1.013×10^5 Pa
p_l = pressure in the fiber lumen, Pa
p'_{O_2} = oxygen partial pressures in the shell side, Pa
p''_{O_2} = oxygen partial pressures in the lumen side, Pa
p_s = pressure in the shell side of the module, Pa
p_v = operating vacuum level, Pa
R = gas constant, 8.314 J mol^{-1} K^{-1}
R_{in} = inner radius of hollow fiber, m
R_o = outer radius of hollow fiber, m
T = operating temperature, K
T_s = setting value of the operating temperature, °C
t = time for measurement, s
V = volume of the test cylinder, m^3
x_e = oxygen concentration in air effluent, %
y_e = oxygen concentration in argon effluent, %
μ = oxygen viscosity, Pa·s
v_l = volumetric flow rate of the lumen gas stream, m^3/s
v_s = volumetric flow rate of the shell gas stream, m^3/s

Literature Cited

1. Kharton VV, Yaremchenko AA, Kovalevsky AV, Viskup AP, Naumovich EN, Kerko PF. Perovskite-type oxides for high-temperature oxygen separation membranes. *J Membr Sci*. 1999;163:307-317.
2. Ullmann H, Trofimenko N. Composition, structure and transport properties of perovskite-type oxides. *Solid State Ionics*. 1999;119:1-8.
3. Dyer PN, Richards RE, Russek SL, Taylor DM. Ion transport membrane technology for oxygen separation and syngas production. *Solid State Ionics*. 2000;134: 21-33.
4. Li S, Jin W, Xu N, Shi J. Synthesis and oxygen permeation properties of $La_{0.2}Sr_{0.8}Co_{0.8}Fe_{0.2}O_{3-\delta}$ membranes. *Solid State Ionics*. 1999;124: 161-170.
5. Stefan D, Herle JV. Oxygen transport through dense $La_{0.6}Sr_{0.4}Fe_{0.8}Co_{0.2}O_{3-\delta}$ perovskite-type permeation membranes. *J Eur Ceram Soc*. 2004;24:1319-1323.
6. Xu SJ, Thomson WJ. Oxygen permeation rates through ion-conducting perovskite membranes. *Chem Eng Sci*. 1999;54:3839-3850.
7. Abrutis A, Teiserskis A, Garcia G, Kubilius V, Saltyte Z, Salciunas Z, Faucheux V, Figueras A, Rushworth S. Preparation of dense, ultra-thin MIEC ceramic membranes by atmospheric spray-pyrolysis technique. *J Membr Sci*. 2004;240:113-122.
8. Teraoka Y, Honbe Y, Ishii J, Furukawa H, Moriguchi I. Catalytic effects in oxygen permeation through mixed-conductive LSCF perovskite membranes. *Solid State Ionics*. 2002;152:681-687.
9. Lee KS, Lee S, Kim JW, Woo SK. Enhancement of oxygen permeation by $La_{0.6}Sr_{0.4}CoO_{3-\delta}$ coating in $La_{0.7}Sr_{0.3}Ga_{0.6}Fe_{0.4}O_{3-\delta}$ membrane. *Desalination*. 2002;147:439-444.
10. Lee S, Lee KS, Woo SK, Kim JW, Ishihara T, Kim DK. Oxygen-permeating property of $LaSrBFeO_3$ (B = Co, Ga) perovskite membrane surface-modified by $LaSrCoO_3$. *Solid State Ionics*. 2003;158: 287-296.
11. Li SG, Jin WQ, Huang P, Xu, NP, Shi J, Lin YS. Tubular lanthanum cobaltite perovskite type membrane for oxygen permeation. *J Membr Sci*. 2000;166:51-61.

12. Wang H, Wang R, Liang DT, Yang W. Experimental and modeling studies on $Ba_{0.5}Sr_{0.5}Co_{0.8}Fe_{0.2}O_{3-\delta}$ (BSCF) tubular membranes for air separation. *J Membr Sci*. 2004;243:405-415.
13. Tan X, Liu S, Li K. Preparation and characterization of inorganic hollow fiber membranes. *J Membr Sci*. 2001;188:87-95.
14. Liu S, Tan X, Li K, Hughes R. Preparation and characterisation of $SrCe_{0.95}Yb_{0.05}O_{2.975}$ hollow fibre membranes. *J Membr Sci*. 2001;193: 249-260.
15. Luyten J, Buekenhoudt A, Adriansens W, Cooymans J, Weyten H, Servaes F, Leysen R. Preparation of $LaSrCoFeO_{3-x}$ membranes. *Solid State Ionics*. 2000;135:637-642.
16. Tan X, Li K. Modeling of air separation in a LSCF hollow-fiber membrane module. *AIChE J*. 2002;48:1469-1477.

Manuscript received Oct. 29, 2004, and revision received Dec. 4, 2004.